Journal of Engineering Research

Volume 9
Issue 1 *issue 1*

Article 18

# Non-Linear Analysis of Axially Loaded Built-Up Open Section Cold-Formed Columns

mai mohamed sheta
*Department of construction and building Engineering, Higher Institute for Engineering, 6th of October City, Egypt*, maisheta39@gmail.com

Hanan Hussein Eltobgy
*Department of Civil Engineering, Faculty of Engineering at Shoubra, Benha University, Egypt*, hanan.altobgy@feng.bu.edu.eg

Mohamed Massoud El Saadawy
*Housing and Building National Research Center (HBRC),87El Tahrir St., Dokki, Giza11511, POBox1770, Cairo, Egypt*, m_massoud2002@yahoo.com

Khaled abdallah Gharib
*Department of Civil Engineering, Faculty of Engineering at Shoubra, Benha University, Egypt*, khaled.Gharib@feng.bu.edu.eg



## Recommended Citation

sheta, mai mohamed; Eltobgy, Hanan Hussein; El Saadawy, Mohamed Massoud; and Gharib, Khaled abdallah () "Non-Linear Analysis of Axially Loaded Built-Up Open Section Cold-Formed Columns," *Journal of Engineering Research*: Vol. 9: Iss. 1, Article 18.
DOI: https://doi.org/10.70259/engJER.2025.911908
Available at: https://digitalcommons.aaru.edu.jo/erjeng/vol9/iss1/18

Journal of Engineering Research (JER)
ISSN: 2356-9441 Vol. 9 – No. 1, 2025 ©Tanta University, Faculty of Engineering e ISSN: 2735-4873

# Non-Linear Analysis of Axially Loaded Built-Up Open Section Cold-Formed Columns

Mai M.Sheta[1*], Hanan H. Eltobgy[2], Mohamed M. El-Saadawy[3], and Khaled A. M. Gharib[4]
[1] Department of construction and building Engineering, Higher Institute for Engineering, 6th of October City, Egypt
[2]Department of Civil Engineering, Faculty of Engineering at Shoubra, Benha University, Egypt
[3]Housing and Building National Research Center (HBRC),87El Tahrir St., Dokki, Giza11511, POBox1770, Cairo, Egypt
[4]Department of Civil Engineering, Faculty of Engineering at Shoubra, Benha University, Egypt
*Corresponding author's email: maisheta39@gmail.com

***Abstract*- Built-up open cold-formed sections are commonly used in entrances, structural corners, and window frames. These elements exhibit low torsional stiffness and are highly susceptible to cross-sectional deformation. Battened built-up cold-formed steel (CFS) open columns offer enhanced load-carrying capacity when individual profiles cannot withstand applied loads. Extensive research has focused on understanding the buckling behavior of these structural elements. However, limited studies have explored the impact of spacing between cold-formed C-channel sections. Existing research suggests that battened columns with adequately spaced members exhibit superior structural performance compared to those with closely spaced channels. A critical factor affecting the performance of battened columns is the slenderness ratio of the unsupported length (Lz) between batten plates. Despite its significance, this aspect has been insufficiently explored in prior studies. The literature lacks defined limiting values for different column slenderness ratios, back-to-back distances between channel sections, and unsupported lengths between batten plates. Consequently, design methods proposed by various researchers may be unreliable. This study investigates the performance of axially loaded pin-ended columns, comprising two appropriately spaced lipped C-channels arranged back-to-back to form open built-up sections. Finite element models were developed using the ABAQUS platform and validated against test results from the literature. Following validation, the models were used for a comprehensive parametric analysis by varying key parameters, such as back-to-back distance, depth-to-width ratios, number of battens, column slenderness ratios, and the relative slenderness of unsupported chords. The study provides a detailed evaluation of how these parameters influence the structural performance of battened columns, offering valuable insights for design optimization and performance assessment.**

***Keywords*- Finite element numerical simulation; battened columns; back-to-back lipped channels; ABAQUS; Steel Built-up c-channel column; Buckling; (CFS) Cold-formed steel column; Axial Load-bearing capacity; Direct Strength Method (DSM) ;Distortional Buckling; Local Buckling**

## I. INTRODUCTION

The finite element (FE) method is widely regarded by engineers as a crucial tool for parametric studies, particularly in modelling cold-formed structural members. Numerous studies have employed multi-point constraints (MPC) in ABAQUS to simulate fasteners connecting cold-formed steel (CFS) elements [1, 2, 3, 4]. Due to their high axial strength, built-up columns are frequently used in construction to enhance structural efficiency. Fasteners such as bolts, screws, welds, and rivets are employed to join individual CFS sections, forming built-up sections that serve as primary load-bearing components. These built-up sections can achieve greater axial compression capacity than separate channel sections when composite action occurs. Self-drilling screws, in particular, are advantageous as they reduce labour time and eliminate the need for pre-drilling. Extensive research has explored the buckling behaviour of axially loaded CFS components. Chen et al. [5] conducted experimental studies to assess various buckling modes of CFS-lipped channel members, focusing on local-distortional buckling and its impact on post-buckling behaviour and ultimate strength. Roy et al. [6] examined built-up

Journal of Engineering Research (JER)
ISSN: 2356-9441 Vol. 9 – No. 1, 2025 ©Tanta University, Faculty of Engineering e ISSN: 2735-4873

steel columns with varying back-to-back distances between sections under axial loads. They found that increasing the vertical distance between connecting channels reduced the columns' load-bearing capacity, especially in medium and slender columns compared to stout and short columns. Roy et al. [7] performed experimental and analytical studies on self-drilling screw connections fastened built-up columns, developing equations to predict their reduced axial strength. El-Aghoury et al. [8] investigated box-section battened columns made of four angles connected by batten plates. They analyzed different column lengths and slenderness ratios (λchord/λ values of 0.67, 1.67, and 2.6) and recommended maintaining λchord/λ ≤ 0.5, not exceeding 0.75 for back-to-back CFS components. Anbarasu [9] experimentally studied CFS-lipped four-angle battened columns with varying lengths and slenderness ratios (λ ranging from 20 to 40, and λchord/λ between 0.35 and 0.64). The study concluded that the λchord/λ ratio significantly influenced column performance, recommending lower values. The research also found that capacity predictions from NAS [10] and EC3 [11] were conservative. Kherbouche et al. [12] demonstrated the superior performance of closed built-up CFS sectional configurations. Dar et al. [13] conducted numerical investigations on CFS battened columns with two channels, evaluating the impact of changes in λsection (30 and 80) and λ (20 to 180). They found that strength estimates for short columns were overly optimistic based on NAS [10] and EC3 [11]. Vijayananad and Anbarasu [14,15] carried out numerical studies on lipped channel CFS battened columns and developed design guidelines, though only limited parameters were examined. This study employs finite element modelling (FEM) to simulate the behaviour of battened columns constructed from double-lipped C-channel sections, forming built-up open cold-formed steel (CFS) configurations joined with self-drilling screws. These built-up sections exhibit significant potential for superior load-bearing capacity compared to conventional single-section components. To validate the developed FEM, its results were compared against experimental test data from the literature on battened columns made of built-up CFS sections. Upon validation, the FEM was employed in a parametric analysis of built-up cold-formed steel (BCFS) battened columns. Based on the numerical findings, the study proposes enhanced design guidelines to investigate the influence of key parameters on structural behaviour, such as back-to-back spacing and slenderness ratio, along with other sectional dimensions. These guidelines aim to ensure accurate and reliable predictions for the load-carrying capacity and failure modes of CFS battened columns.

## II. FE Model investigation

### A. *General description*

A non-linear finite element using ABAQUS [2] was employed to create a numerical model that simulates the behavior of a cold-formed steel battened column, incorporating both its elastic and plastic responses. This model aims to develop a dependable simulation of the behavior of battened columns made from built-up cold-formed steel (BCFS).

The following analysis section delineates the model's geometry and the material properties.

Buckling analysis using finite element methods necessitates two phases of evaluation. The initial phase entails identifying the analysis of the columns` buckling modes of shapes by Eigenvalue. The elastic linear analysis utilizes the (*BUCKLE) command from the library of the ABAQUS, with the applied load during a designated step. This analysis evaluates multiple buckling modes, from which the most pertinent mode identified by the Eigenvalue analysis is chosen. The second stage involves a nonlinear load-displacement analysis considering initial imperfections and nonlinearity of the material. This thorough analysis identifies the columns' ultimate capacity, strains, axial shortenings, failure modes of shape and lateral displacement. .

### B. *Finite element mesh and materials modeling*

For simulation, each detailing of the cold-formed section included end-loading plates, batten plates, and CFS channels in the ABAQUS finite element program using the S4R shell element from the ABAQUS library.

Every node within this shell element in the ABAQUS program has 6 degrees of freedom and is used in various fields. Modelling the lower and upper-end plates was accomplished with a refined mesh of three-dimensional four-node bilinear rigid quadrilateral shell elements (R3D4) from the library of ABAQUS elements.

Convergence methodologies studies were conducted to identify the optimal mesh that ensures sufficient accuracy while minimizing computational time modeling cold-formed steel built-up section battened columns. A fine mesh size of 5 × 5 mm as (length × width) yielded satisfactory accuracy in modeling the built-up section columns, with a finer mesh employed at the corners as illustrated in Fig. 1. A reference point was established at a perpendicular distance from the plane of each end plate, orientated towards the center of the plate, as depicted in Fig. 1.



https://digitalcommons.aaru.edu.jo/erjeng/vol9/iss1/18
DOI: https://doi.org/10.70259/engJER.2025.911908

Journal of Engineering Research (JER)
ISSN: 2356-9441 Vol. 9 – No. 1, 2025 ©Tanta University, Faculty of Engineering e ISSN: 2735-4873

The reference points delineate the effective length of each specimen between the two articulated supports. The boundary conditions were applied to the RPs, while the load was designated to the RP of the upper-end plate. The top loading plate is modeled for the cold-formed steel C-channels using a "Tie" constraint in ABAQUS during the loading method. This command ensures that the rotations and displacements of the linked parts stay constant throughout the loading process. The tie constraint can be employed in ABAQUS [2] to connect three-dimensional shell meshes with other three-dimensional shell meshes automatically. The stress and strain relationship is simplified and ap proximated as bilinear or idealized finite element ana lysis. This approximation is applied to the cross-section. With its versatile capabilities, ABAQUS allows for using a multilinear stress-strain curve, demonstrating its adaptability to handling various material behaviors. This parametric study examined carbon steel properties. Steel is modeled as von misses isotropic hardening, with a minimum yield (Fy) of 355 MPa and an ultimate strength (Fu) of 510 MP a. We used 81000 MPA for shear modulus. Steel is simulated using the bilinear elastic-plastic stress-strain curve. The linear elastic part of the curve used Young's modulus of Eo = 210 GPa an d Poisson's ratio of 0.3. The nonlinear analysis of the model expands isotopically with plastic hardening from a Von Mises-criterion-isotropic yield surface.

### *C. loads and Boundary conditions fastener and contact modelling*

A finite element analysis employing the ABAQUS software program was developed to simulate the behavior of pin-ended built-up columns with cold-formed sections.
Figure 1 demonstrates the implementation of displacements and rotations (boundary conditions) at the upper and lower reference points (RPs) to repli cate the pin-ended supports.

The CONN3D2 element is characterized as a three-dimensional beam connector featuring two nodes and six degrees of freedom per node were employed to represent the self-drilling screws [16,17, 18], as illustrated in Figure 1

The analysis procedure mirrored methodologies used in comparable prior studies [22].The columns were prevented from being translated in the X- and Y-directions and from rotating in the Z-axis in the upper point of the columns.
The column end conditions were constrained against translations in the X, Y, and Z axis and rotation in the Z direction, as illustrated in Figure 2.

A load was applied to the force at the end plate RP. In order to apply the load
in stages, a modified version of the RIKS technique found in the ABAQUS [2] library was utilized.This column examination under axial compressive force (pu) employs the specified loading and boundary conditions.

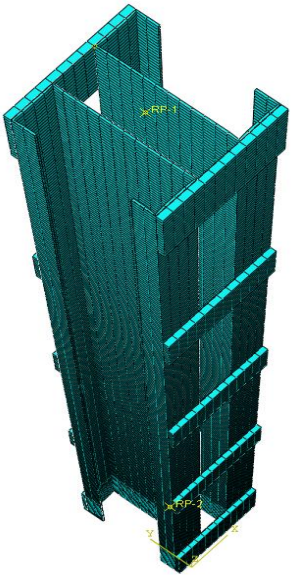


**Load positions**

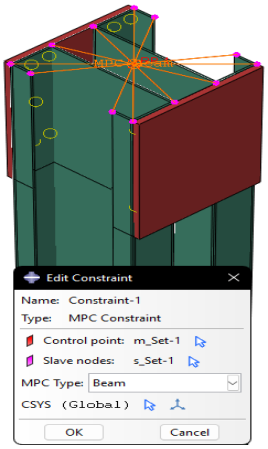


**MPC**

Journal of Engineering Research (JER)
ISSN: 2356-9441 Vol. 9 – No. 1, 2025 ©Tanta University, Faculty of Engineering e ISSN: 2735-4873

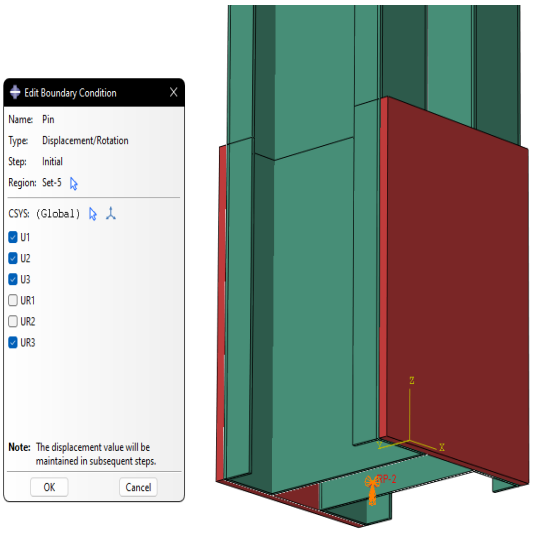


Boundary conditions meshing

a) Finite elements mesh, load application, and Boundary condition

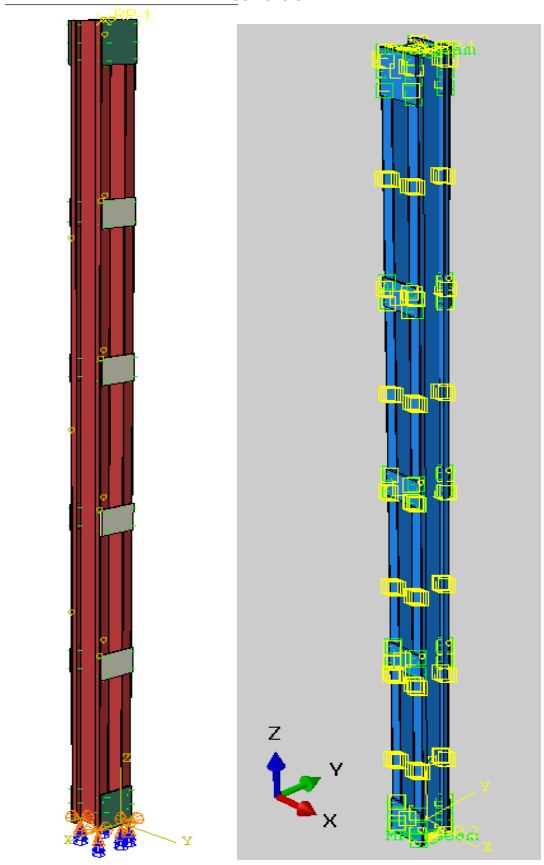


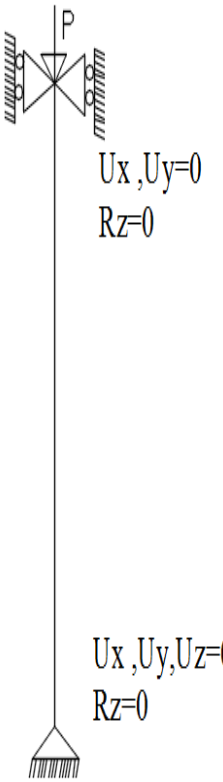


b) Interconnector bolts & arrangement of bolts

Figure1. Numerical modeling a) Finite elements mesh, load application, and Boundary condition b) arrangement of bolts

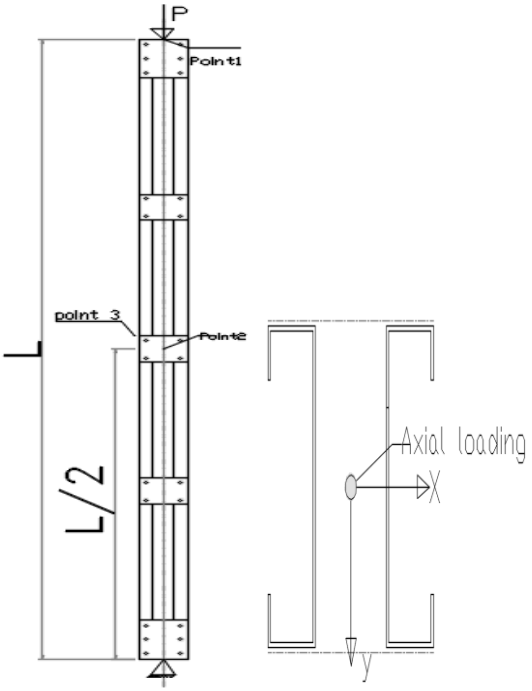


Figure2.Loading positions at column upper loaded end and support position at column lower support end for column subjected to axial and Uni-axial loads.



https://digitalcommons.aaru.edu.jo/erjeng/vol9/iss1/18
DOI: https://doi.org/10.70259/engJER.2025.911908

Journal of Engineering Research (JER)
ISSN: 2356-9441 Vol. 9 – No. 1, 2025 ©Tanta University, Faculty of Engineering e ISSN: 2735-4873

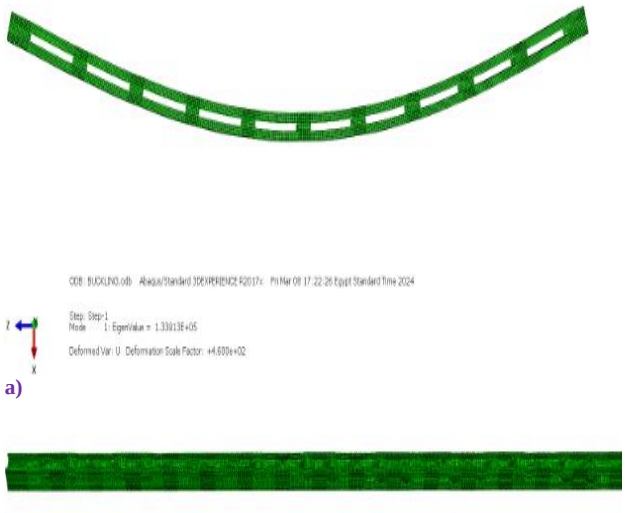

a)

b)

**Figure3. Initial geometric imperfection modes (Eigen mode 1) for a 4.6m built-up column. (a) Overall buckling and (b) Local buckling.**

### *D. Initial geometric imperfections*

The analyzed finite elements consider the observed magnitudes of both failure modes: local buckling and overall buckling.

Eigenvalue analyses of the column can be performed to ascertain the buckling modes and delineate the overall imperfections. The literature review [20] indicates that the average overall imperfections for the tested specimens were determined to be 1/1000 of the total length of the specimen. Imperfections were simulated in battened columns fabricated from assembled cold-formed steel sections. All buckling modes forecasted by the ABAQUS [2] Eigenvalue analysis are standardized to 1.0, Moreover, the value of the overall geometric and initial local imperfections was measured in the buckling modes, as seen in Figure 3.

### *E. Verification of the developed Finite Element Model*

To evaluate the accuracy of the finite element model using ABAQUS [2] in simulating the actual behavior of CFS material, the outcomes of three experimental tests documented in Dabaon [20] conducted experimentally cold-formed built-up C sections, indicating that all factors, including the overall slenderness ratio λ ranging from (50 to 110) and the factor λchord/λ, influenced the performance of battened columns, which were compared with the outcomes of the present finite element model.

The correlations among deformed shape, load vs lateral displacement, and load versus axial shortenin g were analyzed compared to the test results, as sho wn in Fig. 4. Table 1 demonstrates a satisfactory correlation between the experimental ultimate loads and the corresponding values of the current finite element model.

The analysis of the Finite Element Analysis (FEA) results in conjunction with the experimental outcomes across all four dimensions specifically peak strength, failure mode, axial shortening, and the load versus displacement relationship reveals a significant correlation. As a result, the finite element model is well-suited for the proposed parametric studies.

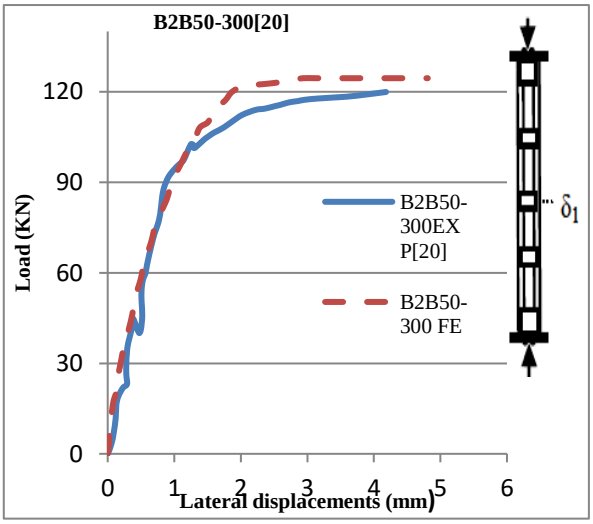


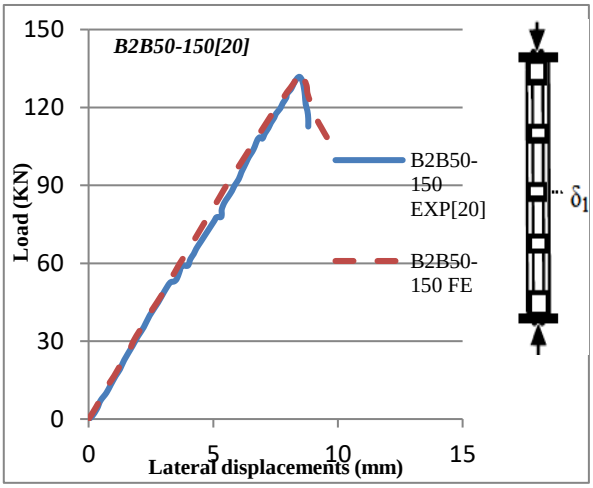


**A) Lateral displacement-load relationships**

Journal of Engineering Research (JER)
ISSN: 2356-9441 Vol. 9 – No. 1, 2025 ©Tanta University, Faculty of Engineering e ISSN: 2735-4873

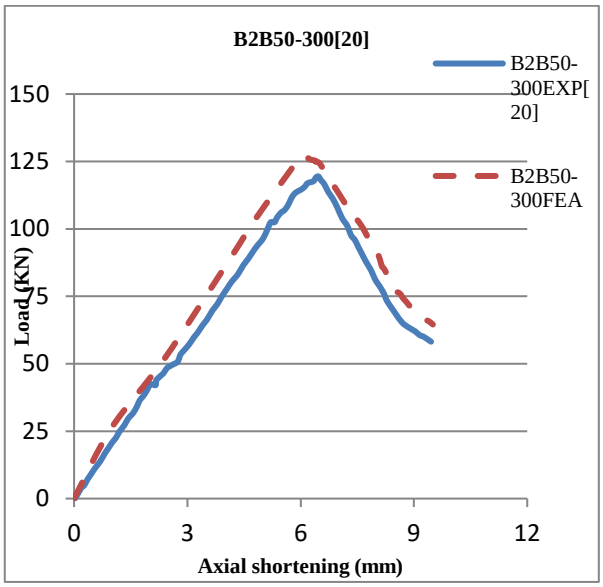


B) Axial shortening -load relationships

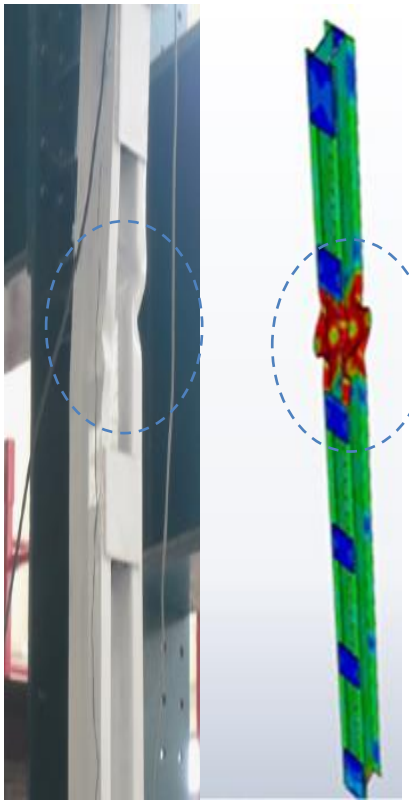

B2B50-300 [20]

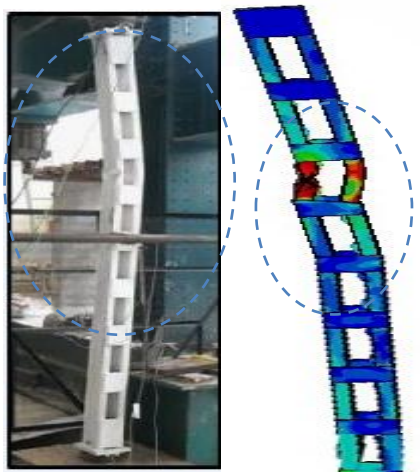

B2B50-150[20]

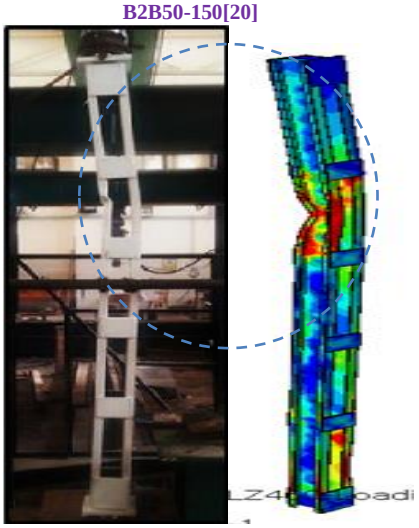

B2B75-300[20]

C) Mode of failure comparison between test specimens and the finite model of [20].

Fig. 4. (A): Lateral displacement-load relationships, (B): Axial shortening, and (C): failure modes Flexural buckling (FB)and local buckling (LB)

Table1. Comparison of the strengths of battened column specimens in FEA and in the experimental test [20].

| Specimen | Ptest (KN) (Exp) | mode of failure (Exp) | P F.E.A (kN) | Failure mode | Ptest/ PF.E.A |
|---|---|---|---|---|---|
| B2B50–300 | 119.11 | FB+LB | 123 | FB+LB | 0.96 |
| B2B75–300 | 125.2 | LB | 126.5 | LB | 0.98 |
| B2B50-150 | 133.12 | FB | 134 | FB | 0.99 |
| Mean | | | | | 0.98 |
| COV | | | | | 0.01 |



https://digitalcommons.aaru.edu.jo/erjeng/vol9/iss1/18
DOI: https://doi.org/10.70259/engJER.2025.911908

Journal of Engineering Research (JER)
ISSN: 2356-9441 Vol. 9 – No. 1, 2025 ©Tanta University, Faculty of Engineering e ISSN: 2735-4873

### *F. Parametric study*

The parametric study analyzed columns with varying back-to-back distances between the two channels (B1) and different buckling lengths (Lz), as shown in Figure 5. A total of 36 columns were evaluated, with dimensions depicted in Figure 5 and listed in Table 2. The column lengths were 2400 mm, 3000 mm, 4600 mm, and 5800 mm, classified into four series based on back-to-back distances (B1) of 40 mm, 60 mm, 80 mm, and 90 mm.

Each column was subjected to axial loading. The buckling lengths (Lz) of single channels within each series were 600 mm, 460 mm, 450 mm, 340 mm, 250 mm, and 175 mm, corresponding to slenderness ratios between batten plates (λz) of 38.7, 29.67, 29.03, 21.93, 16.12, and 11.29, respectively. According to AISI S-100:2016 [10], the overall slenderness ratios (λ = L/rmin) ranged from 50 to 162. Specimen label designations are illustrated in Figure 6.

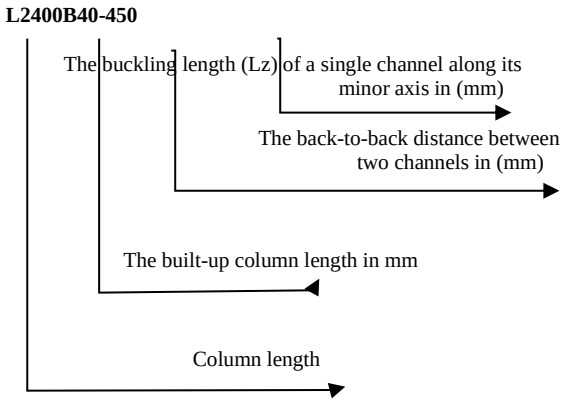


**Fig 6. Label designations of the specimen**

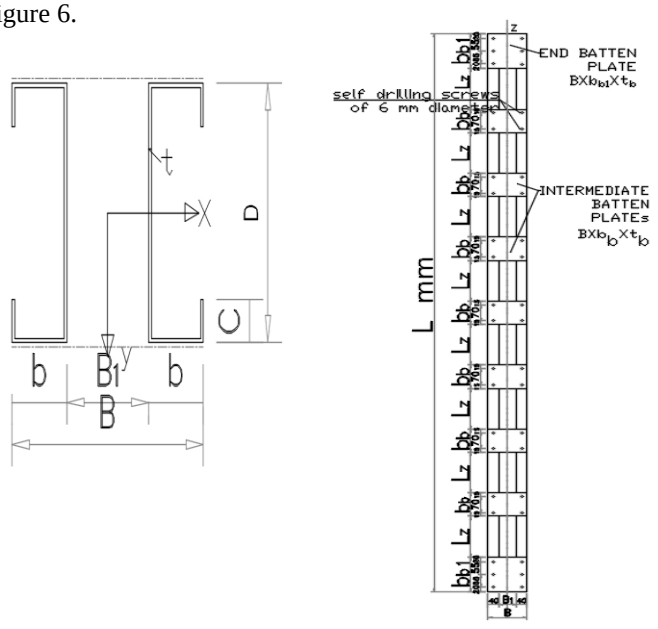


**Fig.5.The cross-sectional dimensions analyzed in the parametric study.**

**Table 2. The parametric study's specimen dimensions:**

| Series | Specimen | L (mm) | Lz (mm) | B1/D | Λz | λ= L/rmin | Channel cross-section in (mm) D × b × c× t | Batten plates' dimensions in (mm) | | |
|---|---|---|---|---|---|---|---|---|---|---|
| | | | | | | | | bb | bb1 | tb |
| B40 | L2400B40-450 | 2400 | 450 | 0.33 | 29.03 | 71.29 | 120 × 40 × 20×2 | 100 | 150 | 6 |
| | L2400B40-340 | 2400 | 340 | 0.33 | 21.93 | 68.71 | 120 × 40 × 20×2 | 100 | 150 | 6 |
| | L2400B40-175 | 2400 | 175 | 0.33 | 11.29 | 66.08 | 120 × 40 × 20×2 | 100 | 150 | 6 |
| | L3000B40-600 | 3000 | 600 | 0.33 | 38.71 | 90.20 | 120 × 40 × 20×2 | 100 | 150 | 6 |

Journal of Engineering Research (JER)
ISSN: 2356-9441 Vol. 9 – No. 1, 2025 ©Tanta University, Faculty of Engineering e ISSN: 2735-4873

| | | | | | | | | | | |
|---|---|---|---|---|---|---|---|---|---|---|
| | L3000B40-460 | 3000 | 460 | 0.33 | 29.67 | 86.60 | 120 × 40 × 20×2 | 100 | 150 | 6 |
| | L3000B40-250 | 3000 | 250 | 0.33 | 16.12 | 82.90 | 120 × 40 × 20×2 | 100 | 150 | 6 |
| | L4600B40-450 | 4600 | 450 | 0.33 | 29.03 | 128.13 | 120 × 40 × 20×2 | 100 | 150 | 6 |
| | L4600B40-340 | 4600 | 340 | 0.33 | 21.93 | 126.70 | 120 × 40 × 20×2 | 100 | 150 | 6 |
| | L4600B40-175 | 4600 | 175 | 0.33 | 11.29 | 125.30 | 120 × 40 × 20×2 | 100 | 150 | 6 |
| | L5800B40-600 | 5800 | 600 | 0.33 | 38.71 | 162.10 | 120 × 40 × 20×2 | 100 | 150 | 6 |
| | L5800B40-460 | 5800 | 460 | 0.33 | 29.67 | 160.13 | 120 × 40 × 20×2 | 100 | 150 | 6 |
| | L5800B40-250 | 5800 | 250 | 0.33 | 16.12 | 158.18 | 120 × 40 × 20×2 | 100 | 150 | 6 |
| B60 | L2400B60-450 | 2400 | 450 | 0.5 | 29.03 | 59.60 | 120 × 40 × 20×2 | 100 | 150 | 6 |
| | L2400B60-340 | 2400 | 340 | 0.5 | 21.93 | 56.49 | 120 × 40 × 20×2 | 100 | 150 | 6 |
| | L2400B60-175 | 2400 | 175 | 0.5 | 11.29 | 53.27 | 120 × 40 × 20×2 | 100 | 150 | 6 |
| | L3000B60-600 | 3000 | 600 | 0.5 | 38.71 | 75.70 | 120 × 40 × 20×2 | 100 | 150 | 6 |
| | L3000B60-460 | 3000 | 460 | 0.5 | 29.67 | 71.50 | 120 × 40 × 20×2 | 100 | 150 | 6 |
| | L3000B60-250 | 3000 | 250 | 0.5 | 16.12 | 67.10 | 120 × 40 × 20×2 | 100 | 150 | 6 |
| | L4600B60-450 | 4600 | 450 | 0.5 | 29.03 | 103.92 | 120 × 40 × 20×2 | 100 | 150 | 6 |
| | L4600B60-340 | 4600 | 340 | 0.5 | 21.93 | 102.16 | 120 × 40 × 20×2 | 100 | 150 | 6 |
| | L4600B60-175 | 4600 | 175 | 0.5 | 11.29 | 100.40 | 120 × 40 × 20×2 | 100 | 150 | 6 |
| | L5800B60-600 | 5800 | 600 | 0.5 | 38.71 | 131.6 | 120 × 40 × 20×2 | 100 | 150 | 6 |
| | L5800B60-460 | 5800 | 460 | 0.5 | 29.67 | 129.26 | 120 × 40 × 20×2 | 100 | 150 | 6 |
| | L5800B60-250 | 5800 | 250 | 0.5 | 16.12 | 126.84 | 120 × 40 × 20×2 | 100 | 150 | 6 |
| B80 | L2400B80-450 | 2400 | 450 | 0.67 | 29.03 | 51.99 | 120 × 40 × 20×2 | 100 | 150 | 6 |
| | L2400B80-340 | 2400 | 340 | 0.67 | 21.93 | 51.94 | 120 × 40 × 20×2 | 100 | 150 | 6 |
| | L2400B80-175 | 2400 | 175 | 0.67 | 11.29 | 51.94 | 120 × 40 × 20×2 | 100 | 150 | 6 |
| | L4600B80-450 | 4600 | 450 | 0.67 | 29.03 | 99.56 | 120 × 40 × 20×2 | 100 | 150 | 6 |
| | L4600B80-340 | 4600 | 340 | 0.67 | 21.93 | 99.56 | 120 × 40 × 20×2 | 100 | 150 | 6 |
| | L4600B80-175 | 4600 | 175 | 0.67 | 11.29 | 99.56 | 120 × 40 × 20×2 | 100 | 150 | 6 |
| B90 | L2400B90-450 | 2400 | 450 | 0.75 | 29.03 | 51.94 | 120 × 40 × 20×2 | 100 | 150 | 6 |
| | L2400B90-340 | 2400 | 340 | 0.75 | 21.93 | 51.94 | 120 × 40 × 20×2 | 100 | 150 | 6 |
| | L2400B90-175 | 2400 | 175 | 0.75 | 11.29 | 51.94 | 120 × 40 × 20×2 | 100 | 150 | 6 |
| | L4600B90-450 | 4600 | 450 | 0.75 | 29.03 | 99.56 | 120 × 40 × 20×2 | 100 | 150 | 6 |
| | L4600B90-340 | 4600 | 340 | 0.75 | 21.93 | 99.56 | 120 × 40 × 20×2 | 100 | 150 | 6 |
| | L4600B90-175 | 4600 | 175 | 0.75 | 11.29 | 99.56 | 120 × 40 × 20×2 | 100 | 150 | 6 |

The ultimate strengths (PFE), failure modes, and non-dimensional critical slenderness (λc) and ($\overline{\lambda}$) of the column, as established by the North American Specification [10] and euro code[11], respectively, are presented in Table 3. Also, the overall slenderness ratio of the column (λ) =L/i min considering the modified length in [10] is listed in Table 2. The relation between (λz) and (λ) studied in this paper is shown in Fig 7.

The results of this parametric research were obtained via the examination of the battened columns finite element model for built-up steel sections. Applying this comprehensive methodology ensures the precision and reliability of our findings.



https://digitalcommons.aaru.edu.jo/erjeng/vol9/iss1/18
DOI: https://doi.org/10.70259/engJER.2025.911908

Journal of Engineering Research (JER)
ISSN: 2356-9441 Vol. 9 – No. 1, 2025 ©Tanta University, Faculty of Engineering e ISSN: 2735-4873

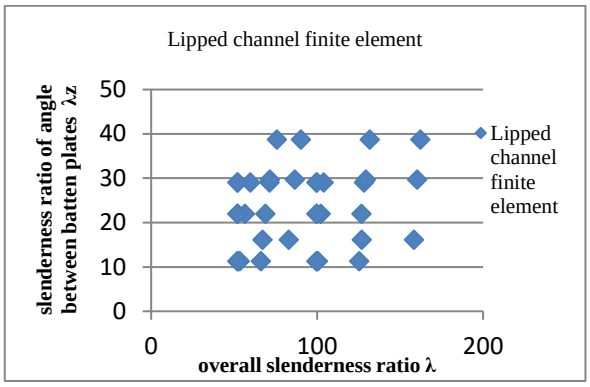


**Fig.7. Critical parameters (λz and λ ) were examined in the study for CFS battened columns made of channels.**

## III. Design rules for built-up columns

### *A. Design rules according to North American (AISI S-100:2016) [10]*

The design code NAS [10] introduces different designs methodologies: the effective width (EWM) and direct strength (DSM) methods and Estimating the elastic critical buckling stress is the primary factor determining the accuracy of DSM. Battened columns are non-prismatic, making elastic critical buckling stress quantification difficult.

**Global buckling and yielding**

Global buckling and yielding refer to the failure mod es of a structural element under the combined effects of flexural, torsional loads, and flexural-torsional.

$$Pne = Ag\ Fn \quad (1)$$

The global compressive stress, Fn, is calculated by the following equation:

$$\begin{cases} Fn = (0.658^{*}\lambda c2)\ fy & for\ \lambda c \le 1.5 \\ Fn = \left(\frac{0.877}{\lambda c^{2}}\right) fy & for\ \lambda c > 1.5 \end{cases} \quad (2)$$

$$Fcre = \frac{\pi 2\ E}{(KL / r)2} \quad (3)$$

The AISI (λc) non-dimensional slenderness ratio is calculated as $\lambda c = \sqrt{(Fy / Fcre)}$,

Fcre denotes the least elastic global buckling stresses pertinent to different modes of shape, such as torsional, flexural, and flexural-torsional.
The symbol (r) indicates the full cross-section radius of gyration about the buckling axis.

$$\lambda mod = \sqrt{\sqrt{\left(\frac{kl}{r}\right)_o^{\ 2} + (\lambda_{chord})^2}} \quad (4)$$

where:
λ mod: the built-up columns modified slenderness ratio
$\frac{kl}{r}$ :the column`s slenderness ratio of the whole cross -section
$\lambda_{chord} : \frac{Lz}{r_i}$ = the slenderness ratio of the chord

**Local buckling in conjunction with global buckling and yielding**

"effective width method"
Pnl = Ae Fn (5)
Calculation of the effective width of each columns can be used to determine Ae.

$$\begin{cases} be = b & where\ \ \lambda 1 \le 0.673 \\ be = b\,/\lambda 1\ (1 - 0.22\,/\lambda 1) & where\ \ \lambda 1 > 0.673 \end{cases} \quad (6)$$

The slenderness factor, λ1, is defined as $\sqrt{(f_n / f_{crl})}$.

$$Fcrl = \frac{\pi^2\ E}{(12(1-\nu^2))\frac{t^2}{b}} \quad (7)$$

"The "direct strength method" is defined in AISI-S100-2016.

$$\begin{cases} Pnl = Pne = Ag\ Fn & for\ \lambda 1 \le 0.776 \\ Pnl = [1 - 0.15\ (Pcrl / Pne)0.4]\ (Pcrl / Pne)0.4\ Pne & for\ \lambda 1 > 0.776 \quad \lambda 1 = \sqrt{(Pne / Pcrl)} \end{cases} \quad (8)$$

**Buckling due to distortion**

$$\begin{cases} Py = Pnd = Ag\ Fy & when \quad \lambda d \le 0.561 \\ Pnd = [1 - 0.25\ (Pcrd / Py)0.6]\ (Pcrd / Py)0.6\ Py & when \quad \lambda d > 0.561 \quad \lambda d = \sqrt{(Py / Pcrd)} \end{cases} \quad (9)$$

$Pcrd = A_g\ f_{crd}$
Pn AISI = the least nominal loads from (pne, pnl and pnd)

### *B. Design regulations according to Eurocode 3, EN 1993-1-3:2006.*

The Euro code (EN 1993-1-1:2006) [11] uses the technique of the effective width of the studied columns for the calculation of the built-up columns' un-factored design strength (PEC3) using the formulae shown below: The class 4 un-factored strength is determined by EC3 (BS EN1993-1-3) as follows:

Journal of Engineering Research (JER)
ISSN: 2356-9441 Vol. 9 – No. 1, 2025 ©Tanta University, Faculty of Engineering e ISSN: 2735-4873

PEC3= $\chi$ AgFy/$\gamma_{m1}$ (For Class1,2 or 3) (10)
=$\chi$AeFy/$\gamma_{m1}$ (ForClass4)

Ae and Ag denote the effective and gross area of the cross-sectional, respectively, defined in euro code [11]sections class 1, 2, 3or4.

Fy represents the yield stress, whereas $\chi$ is the reduct ion factor, which may be computed using Equation ( 11).

$$\chi = (1 / (\varphi + \sqrt{(\varphi^2 - \bar{\lambda}^2)})) \text{ but } \chi \leq 1.0 \quad (11)$$

$$\varphi = 0.5*[1 + \alpha(\bar{\lambda} - 0.2) + \bar{\lambda}^2] \quad (12)$$

The euro code non-dimensional slenderness ratio was calculated as follows:

$$\bar{\lambda} = \sqrt{(AgFy / Ncr)} \text{ (ForClass1, 2 or 3)} \quad (13)$$
$$\bar{\lambda} = \sqrt{(AeFy / Ncr)} \text{ (ForClass4)} \quad (14)$$

$$\bar{\lambda} = (Lcr/i)*((Ae/Ag)/\lambda 1) \quad (15)$$

$$N_{cr,t} = (1 / io^2) [GI_t + \pi^2 EIw / l_T^2] \quad (16)$$

where

Ncr, t the section torsional buckling capacity

Iw: is the constant of warping :$l_T$: the constant of torsional, , and $l_T$ :is the effective length of the torsional.

G : the section shear modulus

$$\lambda_1 = \pi (E/F_y) ^0.5 \quad (17)$$

$$\bar{\lambda} = \text{Maximum}(\bar{\lambda_z}, \bar{\lambda_y}, \bar{\lambda_T})$$

Where:

$\chi$: the applicable buckling mode reduction factor.

Lcr: the buckling length considered.

Ncr: refers to the critical buckling force for elastic design associated with specific buckling mode

Ae: the effective cross-sectional area.

FY: A proof stress of 0.2% ($\sigma$0.2) is the same as the yield stress.

"$\alpha$" imperfection factor.

**Table3. A comparison of the model's strengths and the design's strengths**

| Series | Specimen name | FEM Results | | Different design strength | | | | FE/Code | |
|---|---|---|---|---|---|---|---|---|---|
| | | PuFE (KN) | Failure Mode | PNAS (KN) | $\lambda$c | P EC3 (KN) | $\bar{\lambda}$ | PuFE / PNAS | PuFE /PEC3 |
| B40 | L2400B40-450 | 237.8 | L+D | 233.0 | 0.93 | 232.3 | 0.85 | 1.020 | 1.023 |
| | L2400B40-340 | 241.4 | L+D | 240.0 | 0.89 | 232.3 | 0.85 | 1.005 | 1.038 |
| | L2400B40-175 | 257.8 | L+D | 246.0 | 0.86 | 232.3 | 0.85 | 1.048 | 1.109 |
| | L3000B40-600 | 179.2 | L+D | 177.6 | 1.17 | 176.8 | 1.06 | 1.009 | 1.013 |
| | L3000B40-460 | 188.3 | L+D | 186.1 | 1.13 | 176.8 | 1.06 | 1.011 | 1.06 |
| | L3000B40-250 | 197.5 | L+D | 195.0 | 1.08 | 176.8 | 1.06 | 1.012 | 1.1170 |
| | L4600B40-450 | 106.9 | L+F | 103.5 | 1.67 | 99.9 | 1.63 | 1.033 | 1.070 |
| | L4600B40-340 | 110.0 | L+F | 106.2 | 1.65 | 99.9 | 1.63 | 1.035 | 1.101 |
| | L4600B40-175 | 115.8 | L+F | 108.9 | 1.64 | 99.9 | 1.63 | 1.062 | 1.159 |
| | L5800B40-600 | 55.5 | L+F | 51.1 | 2.12 | 48.7 | 2.05 | 1.087 | 1.139 |
| | L5800B40-460 | 57.8 | L+D+F | 54.4 | 2.09 | 48.7 | 2.05 | 1.062 | 1.185 |
| | L5800B40-250 | 59.0 | L+F | 56.8 | 2.07 | 48.7 | 2.05 | 1.037 | 1.210 |
| B60 | L2400B60-450 | 260.7 | L+D | 260.0 | 0.78 | 266.7 | 0.68 | 1.002 | 0.977 |
| | L2400B60-340 | 269.3 | L+D+F | 267.2 | 0.73 | 266.7 | 0.68 | 1.007 | 1.009 |
| | L2400B60-175 | 276.7 | L+D+F | 274.0 | 0.69 | 266.7 | 0.68 | 1.010 | 1.037 |
| | L3000B60-600 | 218.9 | L+D | 217.6 | 0.99 | 205.4 | 0.85 | 1.005 | 1.065 |
| | L3000B60-460 | 223.9 | L+D | 222.7 | 0.93 | 205.4 | 0.85 | 1.005 | 1.090 |
| | L3000B60-250 | 235.6 | L+D+F | 233.4 | 0.87 | 205.4 | 0.85 | 1.009 | 1.147 |
| | L4600B60-450 | 155.5 | L+F | 154.8 | 1.36 | 142.4 | 1.30 | 1.004 | 1.092 |
| | L4600B60-340 | 161.5 | L+F | 158.9 | 1.33 | 142.4 | 1.30 | 1.016 | 1.134 |
| | L4600B60-175 | 170.3 | L+D+F | 163.0 | 1.31 | 142.4 | 1.30 | 1.044 | 1.196 |



https://digitalcommons.aaru.edu.jo/erjeng/vol9/iss1/18
DOI: https://doi.org/10.70259/engJER.2025.911908

Journal of Engineering Research (JER)
ISSN: 2356-9441 Vol. 9 – No. 1, 2025 ©Tanta University, Faculty of Engineering e ISSN: 2735-4873

| | | | | | | | | | |
|---|---|---|---|---|---|---|---|---|---|
| | L5800B60-600 | 70.9 | L+F | 66.9 | 1.72 | 60.5 | 1.64 | 1.058 | 1.170 |
| | L5800B60-460 | 75.0 | L+D+F | 72.3 | 1.69 | 60.5 | 1.64 | 1.038 | 1.239 |
| | L5800B60-250 | 77.8 | L+F | 76.9 | 1.66 | 60.5 | 1.64 | 1.011 | 1.285 |
| B80 | L2400B80-450 | 277.6 | L+D | 276.7 | 0.68 | 267.0 | 0.67 | 1.003 | 1.039 |
| | L2400B80-340 | 286.3 | L+D | 284.0 | 0.63 | 267.0 | 0.67 | 1.008 | 1.072 |
| | L2400B80-175 | 290.6 | F+D | 276.8 | 0.67 | 267.0 | 0.67 | 1.050 | 1.088 |
| | L4600B80-450 | 167.0 | L+F | 156.1 | 1.30 | 142.8 | 1.30 | 1.069 | 1.169 |
| | L4600B80-340 | 169.8 | L+F | 159.2 | 1.30 | 142.8 | 1.30 | 1.066 | 1.189 |
| | L4600B80-175 | 174.3 | L+F | 164.1 | 1.30 | 142.8 | 1.30 | 1.062 | 1.220 |
| B90 | L2400B90-450 | 285.0 | L+D | 276.8 | 0.679 | 267.0 | 0.67 | 1.029 | 1.067 |
| | L2400B90-340 | 290.6 | F+D | 276.8 | 0.679 | 267.0 | 0.67 | 1.049 | 1.088 |
| | L2400B90-175 | 296.7 | L+D+F | 276.8 | 0.67 | 267.0 | 0.67 | 1.072 | 1.111 |
| | L4600B90-450 | 168.9 | L+D+F | 157.1 | 1.30 | 142.8 | 1.30 | 1.075 | 1.182 |
| | L4600B90-340 | 171.4 | L+D+F | 159.4 | 1.30 | 142.8 | 1.30 | 1.075 | 1.200 |
| | L4600B90-175 | 176.1 | L+D+F | 165.1 | 1.30 | 142.8 | 1.30 | 1.066 | 1.233 |
| Mean Pm = Average of the array (PFEM/Pcode) | | | | | | | | 1.035 | 1.120 |
| Standard deviation | | | | | | | | 0.026 | 0.074 |
| Reliability index, β | | | | | | | | 3.050 | 3.41 |
| Resistance factor, Φ | | | | | | | | 0.850 | 0.850 |

L: local buckling
D; distortion buckling
F: flexural buckling

The results obtained from the analysis of the finite element of the examined (CFS) battened columns are shown in Table 3, which also compared the findings with different analytical computations from many codes. The results indicate that the examined built-up columns with nondimensional slenderness ($\lambda c$) < 0.6 mainly exhibited failure modes distortional (D) and local buckling (L). Conversely, sections with nondimensional slenderness ($\lambda c$) > 1 mostly experienced failure owing to a mix of local buckling (L) and overall flexural buckling (F) failure modes.

## IV. Reliability analysis

The reliability analysis following ASCE Specification [21], aiming for a reliability index (β) of 2.5, as recommended for cold-formed steel (CFS) structural members.

The reliability index (β) was calculated using the load combination 1.2DL + 1.6LL for concentrically loaded compression members, where DL and LL represent dead and live loads, respectively. A capacity reduction factor ($\phi$) of 0.85 was applied per NAS [10] and EC3 [11], with a DL/LL ratio of 0.2.Statistical parameters for the analysis included Mm = 1.10, Fm = 1.00, Vm = 0.10, and VF = 0.05, as specified by ASCE [21]. A correction factor (Cp) was applied to account for the influence of data point quantity on the reliability index, as recommended by NAS [10]. A reliability index above 2.5 indicates a dependable design process, with higher values reflecting greater prediction accuracy. The analysis procedure mirrored methodologies used in comparable prior studies [22].

## V. Discussion of the results

### *A. Failure modes' shape*

For columns subjected to axial loads, three primary failure modes occur due to buckling: local buckling, flexural buckling, and distortional buckling. Table 3 summarizes the maximum load capacities and failure scenarios for each model.

Journal of Engineering Research (JER)
ISSN: 2356-9441 Vol. 9 – No. 1, 2025 ©Tanta University, Faculty of Engineering e ISSN: 2735-4873

71.29 68.71 66.08 90.2 86.6 82.9

L2400 L3000

162.1 160.13 158.18

L5800

(a) Non-linear FE analysis deformed shapes for series B40 with overall slenderness ratio(λ) from (66.08to 162.1)

128.13 126.7 125.3

L4600

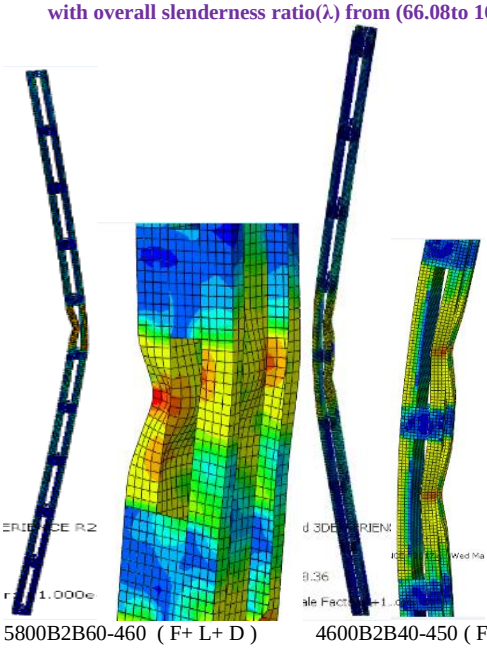

5800B2B60-460 ( F+ L+ D ) 4600B2B40-450 ( F+ L+ D )



https://digitalcommons.aaru.edu.jo/erjeng/vol9/iss1/18
DOI: https://doi.org/10.70259/engJER.2025.911908

Journal of Engineering Research (JER)
ISSN: 2356-9441 Vol. 9 – No. 1, 2025 ©Tanta University, Faculty of Engineering e ISSN: 2735-4873

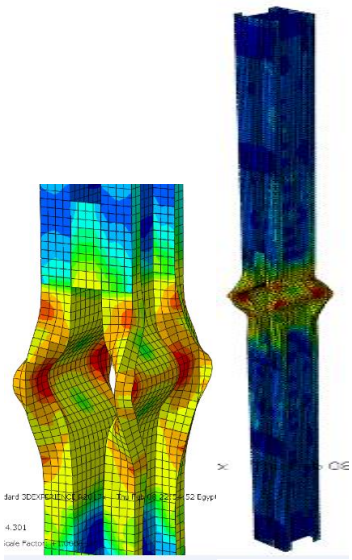

2400b2b40-340 ( L+ D)

b)

**Fig.8.Failure Mode shapes**

In the column model L2400B40-340, which had an ultimate load of 241.4 KN, significant waves of local buckling were observed in the web and flange at failure. The data further indicates that buckling waves appeared in a single channel when the overall slenderness ratio (λ) ranged from 90 to 162.

Notably, models L2400B60-175 and L2400B90-175 exhibited non-linear stress distribution in one channel, as depicted in Fig. 8(b), while stress in the other channel was distributed more linearly.

In contrast, for models L3000B60-340, L3000B60-175, L3000B80-175, and L3000B90-340, an interaction between flexural and distortional buckling was observed, as shown in Fig. 8(a)

In cold-
formed channels, local buckling and distortion distor
tion buckling are similar.

Thus,
a single channel between batten plates has distortion
al or local deformed shapes.

## *B. Comparison between FEA results and design Codes.*

This section compares the finite element (FE) ultimate strength results with the design rules of EC3 [11] and AISI [10], as summarized in Table 3 for axial loads. Axial load capacities were determined using the practical width approach.Figures 10 and 11 illustrate the relationship between the normalized axial load ratio (pu/py) and the non-dimensional slenderness ratios, λc for AISI [10] and $\bar{\lambda}$ for EC3 [11]. Here, pu represents the ultimate load from the finite element analysis, and py is the yield load calculated as the product of the gross cross-sectional area (Ag) and yield stress (Fy) (Py = Ag * Fy). The predicted ultimate loads from AISI [10] and EC3 [11] closely match the FE results, as shown in Figures 10 and 11.The reliability index (β) was maintained between 2.5 and 3.5, ensuring safe and reliable design under various loading conditions. The AISI code incorporates a modified slenderness factor to account for (Lz), as shown in Equation 4. The AISI predictions were more conservative, with safety factors ranging from 1.0028 to 1.07 for axial loads, as shown in Table 3. EC3 predictions had safety factors between 1.00982 and 1.285, showing better alignment with experimental results. The EC3 design provisions account for imperfections and effective widths, particularly for medium-battened columns, where the effects of (Lz) accumulate. The slenderness ratio between batten plates (λz) significantly impacts axial strength. For instance, in columns with a length of 4600 mm and an initial λz of 11.29, increasing λz to 21.9 reduced axial strength by 4%, while further increasing it to 29.03 led to a 30% reduction.Comparisons show that AISI [10] generally provides more conservative results than EC3 [11]. However, in some cases, the FE analysis and design codes yielded highly similar outcomes, as shown in Figure 7 and documented in Table 3.

A notable observation is that as the column back-to-back distance-to-depth ratio (B1/D) decreases, the normalized axial load ratio (PUFE/Py) also decreases across different column lengths. Additionally, for the same B1/D, longer columns exhibited lower PUFE/Py ratios. Overall, the AISI design code showed satisfactory agreement with the FE modeling results for axially loaded columns.

Journal of Engineering Research (JER)
ISSN: 2356-9441 Vol. 9 – No. 1, 2025 ©Tanta University, Faculty of Engineering e ISSN: 2735-4873

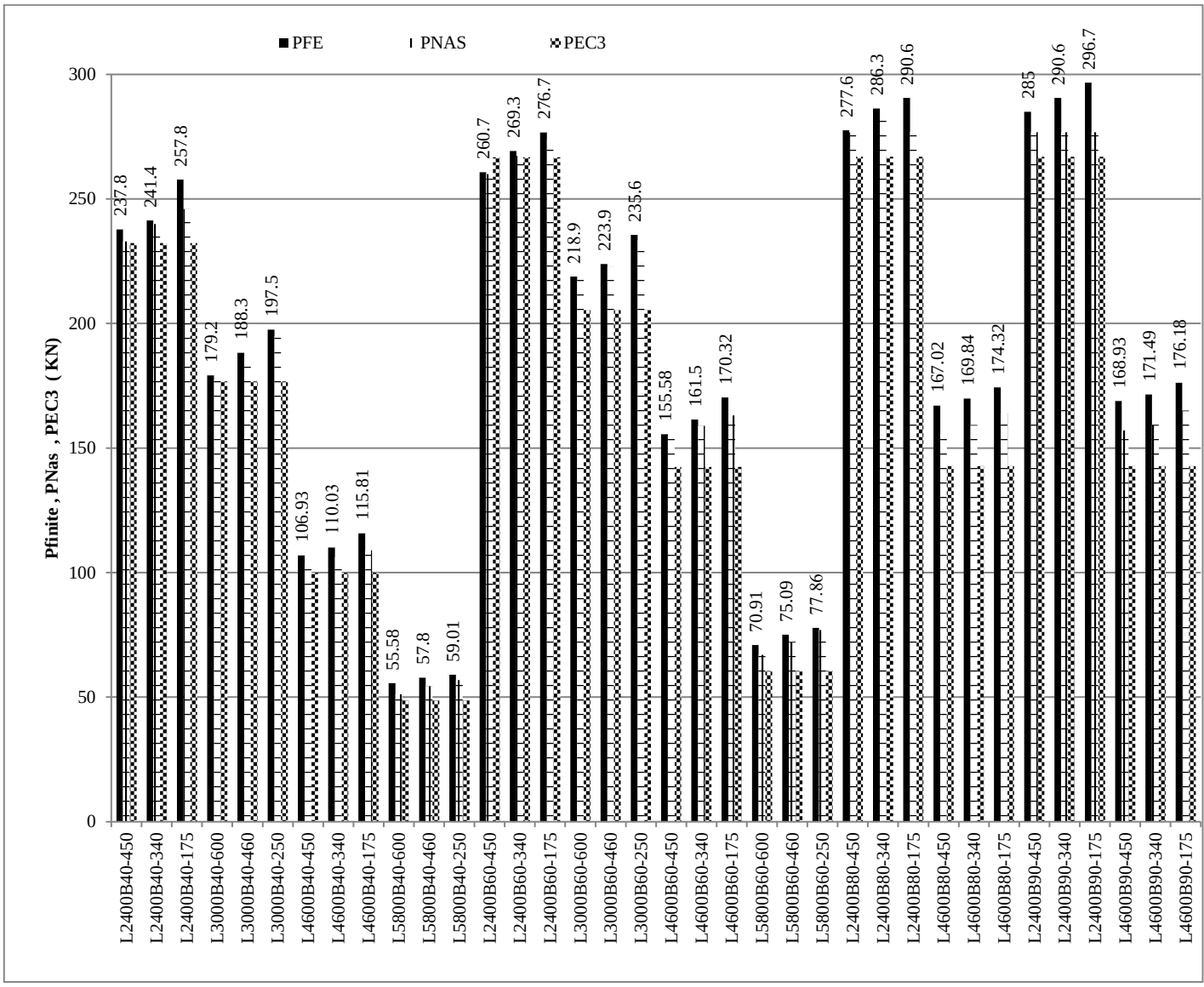


**Figure 9: Comparison between results from the tests with the predictions of the design strength**

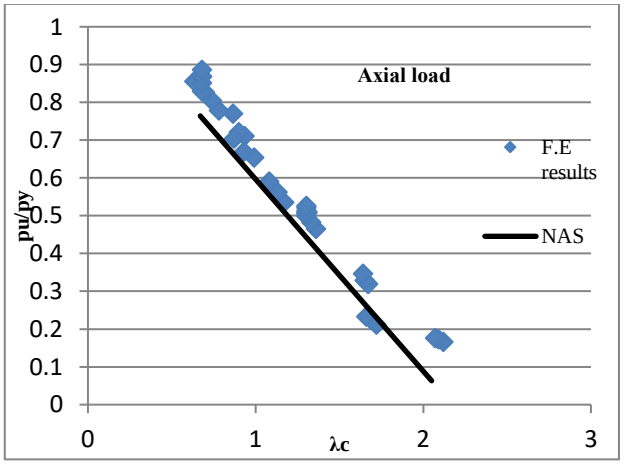


**Fig10. Comparison of the finite element strengths And AISI [31]design code non-dimensional (λc)**

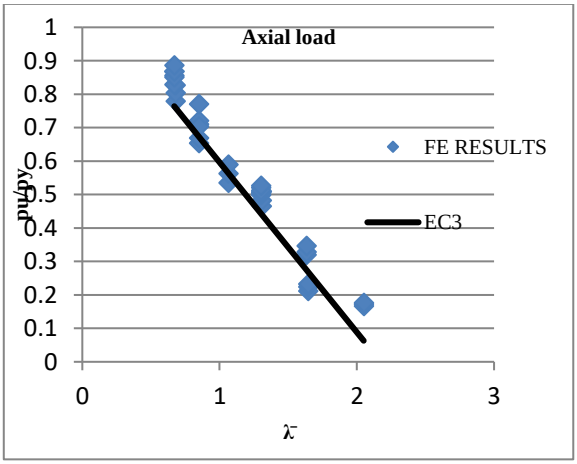


**Fig11.Comparison of the finite element and EC3 [32] design non-dimension slenderness slenderness (λ̄)**



https://digitalcommons.aaru.edu.jo/erjeng/vol9/iss1/18
DOI: https://doi.org/10.70259/engJER.2025.911908

Journal of Engineering Research (JER)
ISSN: 2356-9441 Vol. 9 – No. 1, 2025 ©Tanta University, Faculty of Engineering e ISSN: 2735-4873

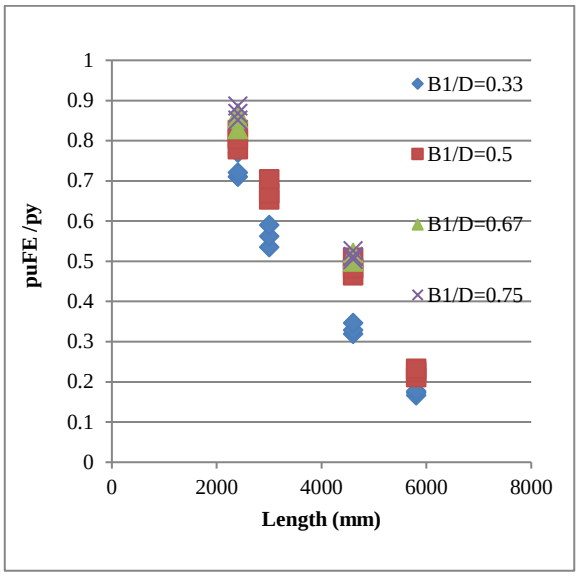


**Fig12. Effect of B1/D ratio for different column lengths on the column capacity**

### C. *Axial shortening versus axial load*

The axial compression magnitude was assessed at point 1, situated at the loaded end of the column, as s een in the finite element in Figure 1.
Figure 13 illustrates the CFS relationship between axial load versus
axial shortening for different models.

The structure consists of columns with varying slenderness ratios of channels between batten plates and overall slenderness ratios. The figure illustrates the relationship between axial shortening and axial load response of columns with the same column depth-to-width ratio (D/B).
The maximum axial strengths of columns decrease a s the overall slenderness ratio increases (λ).
Only a tiny amount of nonlinearity is seen in the plot s of axial load versus axial shortening
before the columns reach their maximum axial stren gths.Furthermore, there is a gradual decrease in the a xial strength observed in the columns after reaching their peak behavior.The columns experienced failure due to a combination of local and global (or flexural ) buckling modes. The columns exhibited the failure modes identified as flexural and local buckling. When the column's depth-to-width ratio (D/B) is less than or equal to 0.75, accompanied by high overall slenderness ratios, a pronounced nonlinear response is seen in the correlation between axial load and axial shortening. For axial columns, the peak axial strength of columns and the axial shortening are influenced by the column depth-to-width ratio (D/B) for the same cross-section. For example, columns having (D/B) of 0.7058 exhibited a reduction in peak axial strengths by 8%, 7.3% and 6.7% for L=2400 and LZ=29.032, 21.935 and11.29 respectively, if the value of (D/B) is increased from 0.7058 to 0.857 and by 14%,13.9 % and11.2% if the value of (D/B) is increased from 0.75 to 1 for lz=450,340 and175 respectively.When comparing models with the same column diameter (D/B) but different loading types, it was
observed that the axially loaded column exhibited gr eater stiffness than the columns
subjected to other loading types.

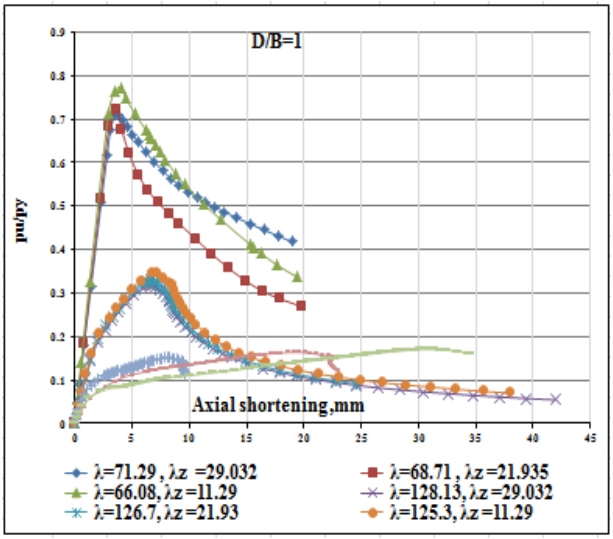


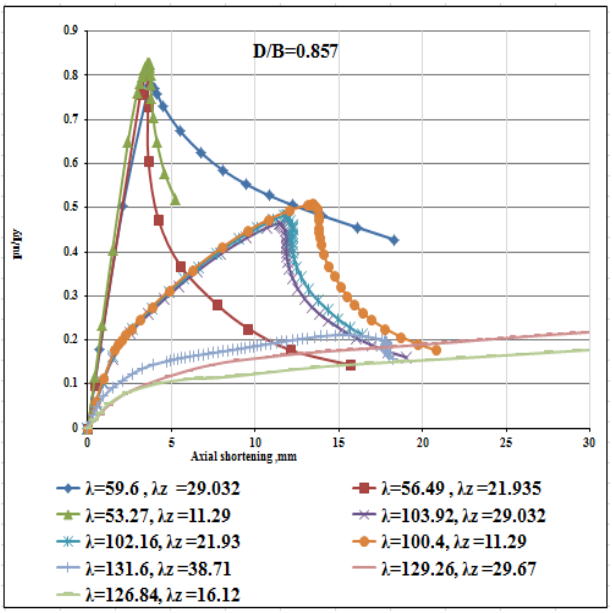

Journal of Engineering Research (JER)
ISSN: 2356-9441 Vol. 9 – No. 1, 2025 ©Tanta University, Faculty of Engineering e ISSN: 2735-4873

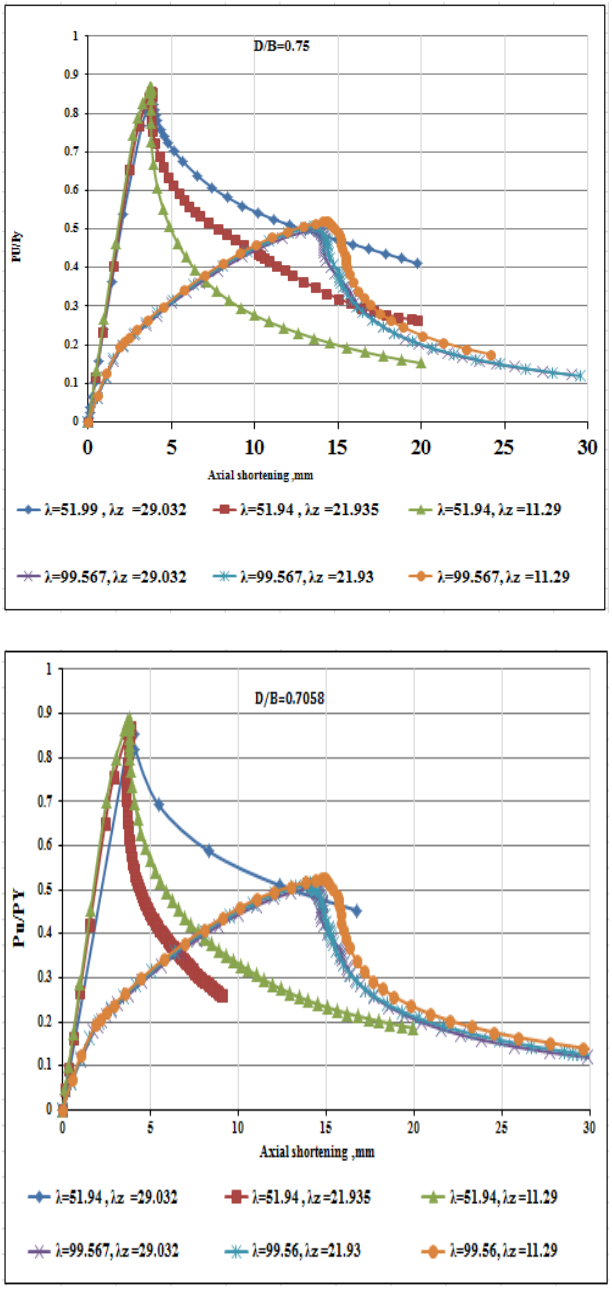


**Figure13:**
**Relationships between load and axial shortening for axially loaded columns**

### *D. Load and lateral displacement (Ux and Uy)*

The lateral displacements were measured at two locations at the midpoint of the model to quantify the displacement in both the X and Y directions. The first location, referred to as"point2," is shown in the figure2. The second location is at the midpoint of the cross-sectional flange and is designated as point 3, as depicted in Figure 2.

In the axially loaded column, the lateral displacement in the x-direction (ux) was more significant than the lateral displacement in the y-direction (uy). The relationship between the axial load and lateral displacement response of columns with different channel slenderness ratios between batten plates (λz) is depicted in Figure 14. Once the short columns reach their peak strength, regarded as insignificant, their axial strength significantly decreases.The column with a higher slenderness ratio exhibited more, excellent ductility than those with a smaller slenderness ratio. Therefore, the ductility of the column was directly correlated with the overall slenderness ratio.The lateral displacements (Δ) at which the columns reached their maximum axial strengths are normalized relative to their length (L).The axial stiffness of a column is evident when it is subjected to axial load, with column dimensions of D/B) = 0.70 and 0.75.

Meanwhile, columns subjected to the axial stiffness were inversely proportional to the overall slenderness ratio for an axial load with the same column depth-to-width ratio (D/B).

Additionally, the axial stiffness of the columns with channel slenderness ratios between batten plates (λz) of 11.29 was higher than that of the columns with slenderness ratios of 21.94 and 29.03.

Due to the absence of stiffeners in the chord members of the built-up columns, which are made of unstiffened CFS channel sections, these columns are prone to local buckling failures. As a result, the normalized lateral displacements of the columns showed a scattered upward trend.Similarly, increasing the channel slenderness ratios between batten plates (λz) leads to higher lateral drift before failure and significantly reduces scattering.



https://digitalcommons.aaru.edu.jo/erjeng/vol9/iss1/18
DOI: https://doi.org/10.70259/engJER.2025.911908

Journal of Engineering Research (JER)
ISSN: 2356-9441 Vol. 9 – No. 1, 2025 ©Tanta University, Faculty of Engineering e ISSN: 2735-4873

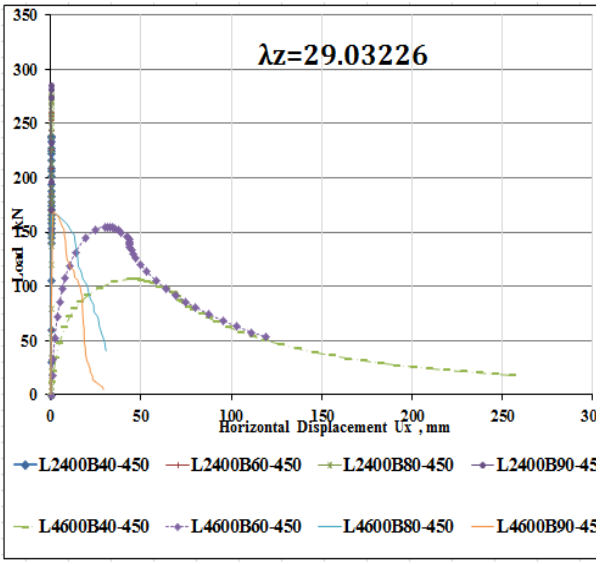


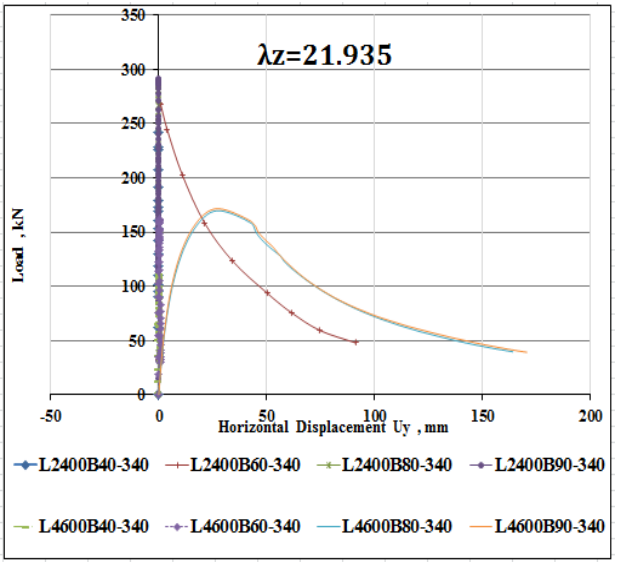


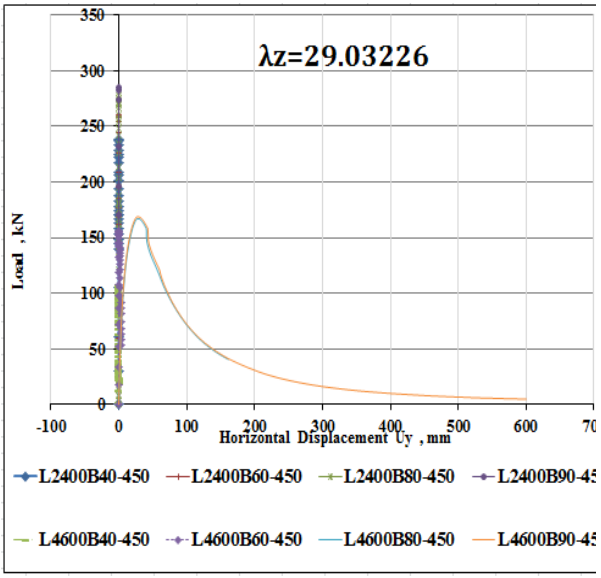


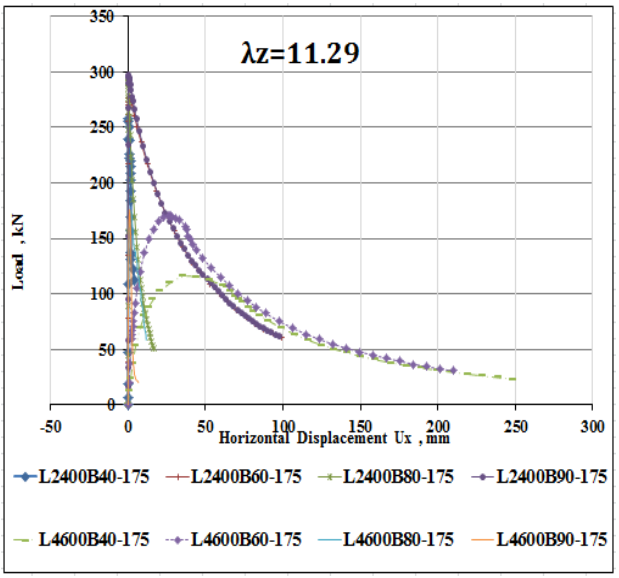


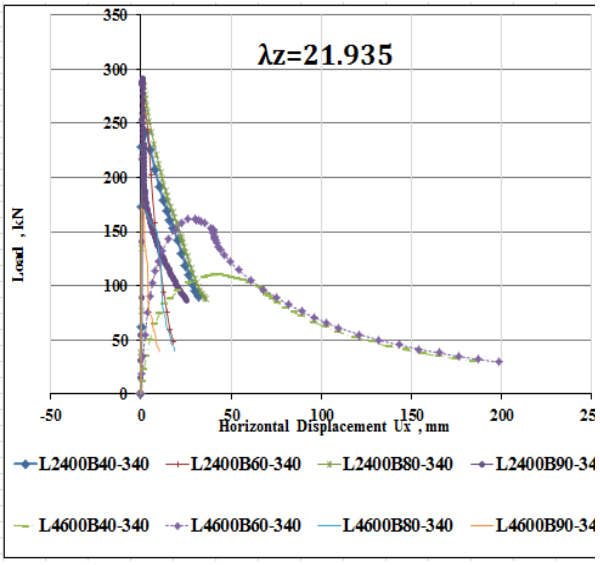


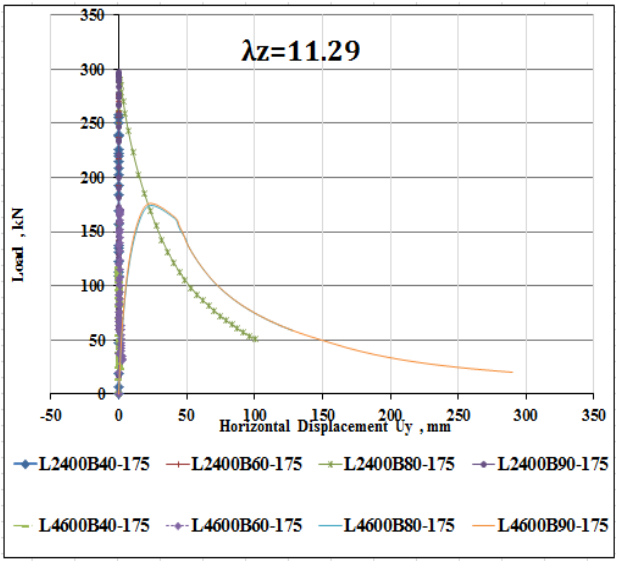

Journal of Engineering Research (JER)
ISSN: 2356-9441 Vol. 9 – No. 1, 2025 ©Tanta University, Faculty of Engineering e ISSN: 2735-4873

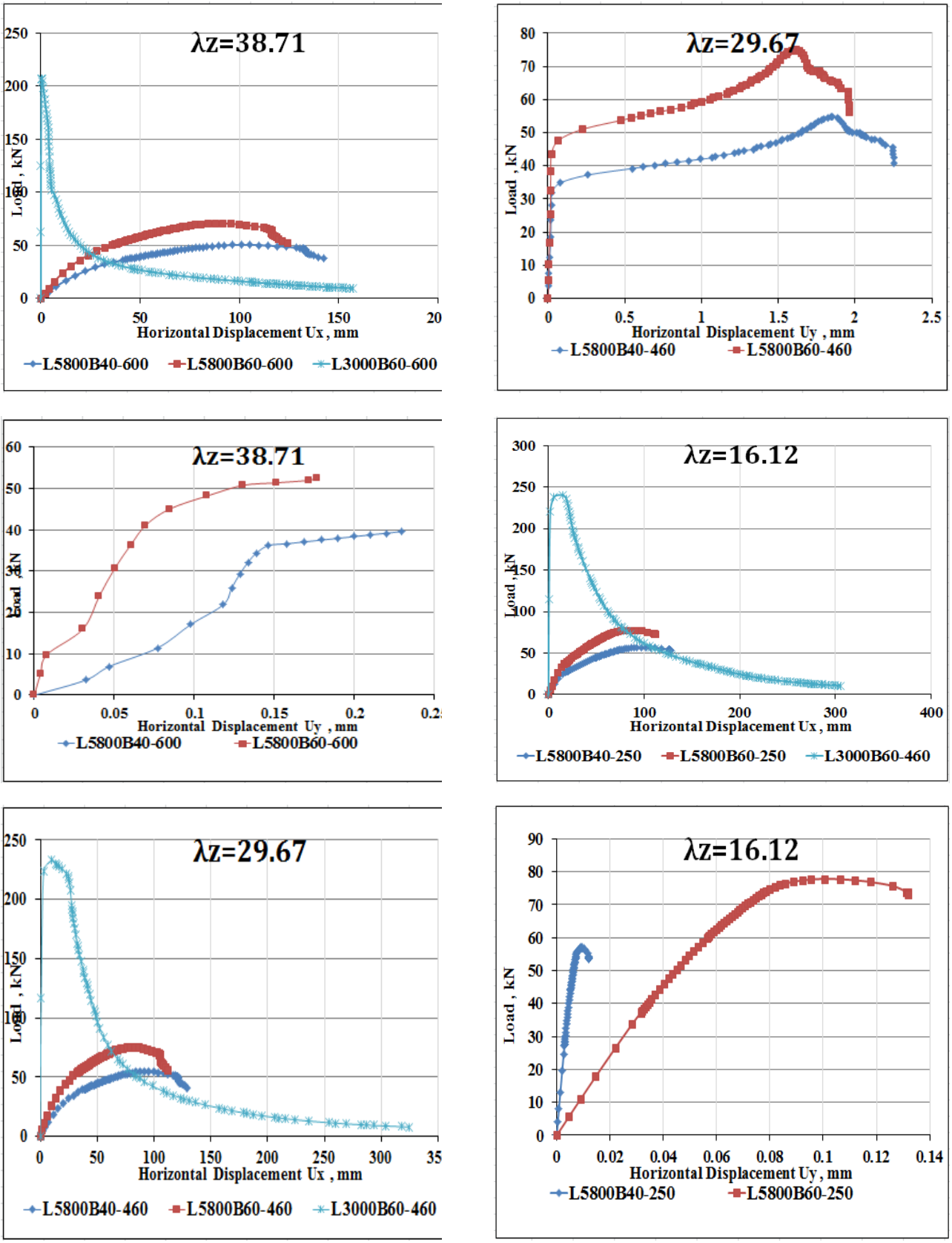


**Figure 14: The relationships between load and lateral displacement (Ux) and (Uy) for columns subjected to a xial loads.**



https://digitalcommons.aaru.edu.jo/erjeng/vol9/iss1/18
DOI: https://doi.org/10.70259/engJER.2025.911908

Journal of Engineering Research (JER)
ISSN: 2356-9441 Vol. 9 – No. 1, 2025 ©Tanta University, Faculty of Engineering e ISSN: 2735-4873

## VI. CONCLUSION

The investigation utilized a nonlinear finite element model to analyze the ultimate capacity of battened columns composed of two thin channel sections arranged in a back-to-back configuration. The models accounted for both geometric and material nonlinearities.

For axially loaded columns, the failure modes varied based on column length:

Short columns: Local buckling was the primary failure mode.
Long columns: Flexural buckling dominated failure.
Intermediate columns: Failure occurred due to interactive buckling (a combination of local and flexural buckling).
Finite element results for short and slender battened columns closely matched EC3 and AISI-LRFD specifications. Medium columns predominantly failed due to local and flexural buckling. For sections with a high slenderness ratio, EC3 and AISI-LRFD predictions were not conservative, with EC3 being less reliable than AISI.

Geometrical imperfections ($\Delta$ = L/1000) were incorporated in all loading cases, including axially loaded members.

Failure behavior varied based on buckling type:

Local buckling: The Direct Strength Method (DSM) provided un-conservative results, while Global buckling: DSM results were slightly conservative.
According to EC3, open sections yielded conservative predictions for local buckling and slightly conservative predictions for global buckling. However, Uniaxially loaded columns demonstrated the opposite behavior.
For column cross-sections with intermediate slenderness ratios ($\lambda c$), the strength reduction exhibited a concave downward relationship, with maximum strength reduction occurring under primarily axial compressive loading.

Furthermore, the ultimate strength was negatively impacted by both the slenderness ratio of channels between batten plates ($\lambda z$) and large back-to-back distances between channel sections.

**Conflicts of Interest:** The authors declare no conflict of interest.

## REFERENCES

[1] D. C. Fratamico and B. W. Schafer, "Numerical studies on the composite action and buckling behavior of built-up cold-formed steel columns," in 22nd International Specialty Conference on Cold-Formed Steel Structures, 2014.
[2] ABAQUS Analysis User's Manual-Version 6.16, USA: ABAQUS Inc., 2016.
[3] C. Yu and B. W. Schafer, "Simulation of cold-formed steel beams in local and distortional buckling with applications to the direct strength method," Journal of Constructional Steel Research, vol. 63, pp. 581-590, 2007.
[4] Y. Li, Y. Li, S. Wang, and Z. Shen, "Ultimate load-carrying capacity of cold-formed thin-walled columns with built-up box and I section under axial compression," Thin-Walled Structures, vol. 79, pp.202-217, 2014.
[5] M.T. Chen, B. Young, A.D. Martins, D. Camotim, P.B. Dinis, "Experimental investigation on cold-formed steel stiffened lipped channel columns undergoing local-distortional interaction," Thin-Walled Struct. 150 (2020) 106682.
[6] Roy, K., Ting, T.C.H., Lau, H.H., Lim, J.B.P. (2018) "Nonlinear behavior of back-to-back gapped built-up cold-formed steel channel sections under compression," Journal on Constructional Steel Research, 147 257-276.
[7] Krishanu Roy, Hieng Ho Lau, et al. "Experiments and finite element modelling of screw pattern of self-drilling screw connections for high strength cold-formed steel," Thin-Walled Structures 145 (2019) 106393.
[8] M.A. El-Aghoury, A.H. Salem, M.T. Hanna, E.A. Amoush, "Experimental investigation for the behavior of battened beam-columns composed of four equal slender angles," Thin-Walled Struct. 48 (9) (2010) 669–683.
[9] M. Anbarasu, "Behavior of cold-formed steel built-up battened columns composed of four lipped angles: tests and numerical validation," Adv. Struct. Eng. 23 (1) (2020) 51–64.
[10] AISI S-100, "North American Specification for the Design of Cold-Formed Steel Structural Members," AISI Standard, Washington, DC, 2016.
[11] EN 1993-1-3, Eurocode 3: "Design of Steel Structures. Design of Steel Structures. Part 1–3: General Rules – Supplementary Rules for Cold-Formed Members and Sheeting ," European Committee for Standardization, Brussels, 2006.
[12] S. Kherbouche, A. Megnounif, "Numerical study and design of thin-walled cold-formed steel built-up open and closed section columns," Eng. Struct. 179 (15) (2019) 670–682.
[13] M.A. Dar, D.R. Sahoo, A.K. Jain, "Influence of chord compactness and slenderness on axial compression behavior of built-up battened CFS columns," J. Build. Eng. 32 (2020), 101743.
[14] S. Vijayanand, M. Anbarasu, "Parametric study and improved design guidelines of CFS battened built-up columns," Steel Compos. Struct. 40 (5) (2021) 733–746.
[15] S. Vijayanand, M. Anbarasu, "Behavior of CFS built-up battened columns: parametric study and design recommendations," Struct. Eng. Mech. 74 (3) (2020) 381–394.
[16] X. Zhou, Y. Xiang, Y. Shi, L. Xu, Y. Zou, "Simplified design method of cold-formed steel columns with built-up box sections," Eng. Struct. 228 (2021), 111532.
[17] S. Nie, T. Zhou, M.R. Eatherton, J. Li, Y. Zhang, "Compressive behavior of built-up double-box columns consisting of four cold-formed steel channels ," Eng. Struct. 222 (2020), 111133.
[18] S. Kechidi, D.C. Fratamico, B.W. Schafer, J.M. Castro, Bourahla., "Simulation of screw connected built-up cold-formed steel back-to-back lipped channels under axial compression ," Eng. Struct. 206 (2020) 110109.
[19] H. Luo, J. Liu, C. Li, K. Chen, M. Zhang, "Ultra-rapid delivery of specialty field hospitals to combat COVID-19: lessons learned from the Leishenshan hospital project in Wuhan," Autom. Constr. 119 (2020), 103345.
[20] M. Dabaon, E. Ellobody, K. Ramzy, "Experimental investigation of built-up cold formed steel section battened columns ," Thin-Walled Struct. 92 (2015) 137–145.

Journal of Engineering Research (JER)
ISSN: 2356-9441 Vol. 9 – No. 1, 2025 ©Tanta University, Faculty of Engineering e ISSN: 2735-4873

[21] ASCE. Minimum design loads for buildings and other structures," ASCE/SEI 7-05.American Society of Civil Engineers Standard; 2006.

[22] M. Adil Dar a, Abhishek Verma b, et al, "Design of cold-formed steel battened built-up columns," Journal of Constructional Steel Research 193 (2022) 107291



https://digitalcommons.aaru.edu.jo/erjeng/vol9/iss1/18
DOI: https://doi.org/10.70259/engJER.2025.911908